Supplementary file 1: Environment determines evolutionary trajectory in a constrained phenotypic space

David T. Fraebel, Harry Mickalide, Diane Schnitkey,
Jason Merritt, Thomas E. Kuhlman, Seppe Kuehn

(Dated: December 22, 2016)

CONTENTS

I. ADDITIONAL SELECTION EXPERIMENTS

We performed selection on the motile but non-chemotactic mutant $\Delta cheA$-Z in the same genetic background used for all other experiments (MG1655-motile). In rich medium, we observed migration an order of magnitude slower than the wild-type and only a small increase in s over 10 rounds of selection (Figure 1 - figure supplement 1). In this experiment each round of selection lasted 24 hours to permit this strain to form colonies large enough for reliable sampling. In minimal medium the non-chemotactic mutant formed no measurable front during 48 hours of incubation and selection, performed by sampling from the periphery of this colony, resulted in only a very small increase in migration rate in one replicate after 7 rounds of selection. For the minimal medium experiment antibiotics were used to limit

the possibility of contamination and the $\Delta cheA\text{-}Z$ deletion was confirmed by PCR.

We performed selection in rich medium where populations were sampled every 12 hours from a point halfway the center of the colony and the outer edge; results are shown in Figure 1 - figure supplement 3. When sampling at this location we observed slower adaptation and a reduction in the maximum rate of expansion compared to populations selected by sampling at the migrating front.

Since previous work has shown that non-genetic diversity can be important in chemotaxis and front migration.[1,2] To test whether the adaptation we observe has a genetic basis, we asked whether long-term growth in liquid culture resulted in loss of the fast migration phenotype. We inoculated a strain isolated after 15 rounds of selection in rich medium (Figure 1(c), main text, replicate 1) into a custom turbidostat that maintained a population of ~10^9 cells under well mixed and constant temperature conditions. We inoculated soft agar plates from this continuous culture at regular intervals over approximately 140 generations of growth in liquid culture. We observed no decrease in the rate of migration due to prolonged growth in liquid culture (Figure 1 - figure supplement 5), suggesting that non-genetic variation likely does not play a large role in the adaptation we observed.

II. MEASUREMENTS OF GROWTH RATES

Growth rate measurements were performed using custom-built optical density measurement device.[3] Briefly, this device used an infrared LED and a photodetector to measure the transmitted light passing through a culture vial. The LED and photodetector were embedded in an aluminum block that was temperature controlled by a Peltier element and PID feedback software. Strains were inoculated from overnight culture into 20 mL vials of the appropriate medium stirred at 850 rpm and maintained at 30 °C. The growth rate was measured by linear regression of $log(OD(t))$ over a 150 to 200 minute window where the change in OD is determined to be exponential by inspecting the residuals. We checked that the conclusions in Figure 3, Figure 3 - figure supplement 3 and Figure 4 – figure supplement 2 did not depend qualitatively on the time interval used in fitting the optical density curves.

III. NUMERICAL SIMULATIONS OF REACTION-DIFFUSION MODEL

Under the assumptions of vertical uniformity in the plate and azimuthal symmetry, the numerical integration of equations (1) and (2) in the main text was coded in C++ as a one dimensional lattice representing a horizontal line projecting from the center of the plate to the edge. Each lattice site had both a food/attractant density ($c(\mathbf{r},t)$, initially uniform) and a bacterial surface density ($\rho(\mathbf{r},t)$, with an initial inoculum corresponding to 1.4×10^8 cells ml^{-1} at the center). A lattice spacing of 0.15 mm was used with a step time of 0.0625 min; every step the entire system was updated according to the model (in cylindrical coordinates) using standard nearest-neighbor finite difference equations for the first and second derivatives on a lattice. To prevent seeding the far end of the plate with bacteria in nonphysical time, densities greater than 100 cells ml^{-1} were required to seed a lattice site as the bacteria propagated outward. Changing this threshold did not alter the results. The front position was determined by finding the first local maximum in ρ from the edge of the plate. Front velocities were determined via linear fit on front position with time. Examples of simulation outputs are shown in Figure 2 – figure supplement 1. Parameters for our simulation in both rich and minimal medium were either measured or taken from the literature and values are given in Table 11 of the main text.

IV. RELATIONSHIP BETWEEN SINGLE-CELL BEHAVIOR AND FRONT MIGRATION

The relationship between single-cell swimming parameters (v_r, τ_r and τ_t) and population transport parameters (k_0 and D_b) has been described in detail elsewhere.[4–6] Here we summarize the results of these calculations and give details for the estimates given in the main text. Rivero *et al.*[4] considered chemotaxis in one spatial dimension by considering the dynamics of two populations of cells: those moving left and those moving right at constant speed $|v_r|$. They neglect variation in $|v_r|$ across the population and time; they also treat tumbles as instantaneous. They define the probability that a cell swimming to right tumbles and begins swimming to the left as α^+ and the converse as α^-. Under these assumptions they show that

$$D_b = \frac{2v_r^2}{\alpha^+ + \alpha^-} \tag{1}$$

and

$$k_0 = v_r \frac{\alpha^- - \alpha^+}{\alpha^+ + \alpha^-}. \tag{2}$$

Note that the tumble frequency is $\alpha_0 = \alpha^+ + \alpha^-$. As discussed in the main text, Croze *et al.* use this as a starting point for deriving a relationship between the transport parameters D_b and k_0 and the behavioral parameters $|v_r|$ and τ_r. For completeness we give the main results of their derivation here; for further details see Appendix A of reference.[5] First, *E. coli* modifies its tumble frequency in response to environment according to

$$\alpha(t) = \alpha_0[1 - \int_{-\infty}^{t} dt' K(t-t') f_{k_0}(x(t'))] \tag{3}$$

where α_0 is the unstimulated tumble frequency, x is a spatial coordinate and the integral contains the response function (K)[7] and $f_{k_0} = c(x)/(c(x) + K_D)$ describes the binding of an attractant at concentration $c(x)$ to the relevant receptor. Experimentally, it has been shown that $\int_{-\infty}^{\infty} dt K(t) = 0$.[7] We proceed by assuming that the effective tumble frequency due to collisions with the agar can be written as $\alpha_e(t, C) = \alpha(t) + \alpha_A(C)$. The authors then compute an average run duration given $\alpha_e(t, C)$. We note that in this derivation, f_{k_0} is expanded and truncated to first order. The result is

$$D_b(C) = \frac{v_r^2}{\alpha_0} \frac{1}{(1 + \alpha_A(C)/\alpha_0)} \tag{4}$$

and

$$k_0(C) = \frac{v_r^2}{\alpha_0} \frac{1}{(1 + \alpha_A(C)/\alpha_0)^2} \int_0^{\infty} dt K(t) e^{-(\alpha_0 + \alpha_A(C))t} \tag{5}$$

For k_0 the authors approximate the integral when $\alpha_A(C) \approx \alpha_0$ (the 'efficient limit') to $\int_0^{\infty} dt K(t) e^{-(\alpha_0+\alpha_A(C))t} \approx 1 - \kappa\alpha_A(C)/\alpha_0$ with $\kappa = \int_0^{\infty} dt' \alpha_0 t' K(t') e^{-\alpha_0 t'} / \int_0^{\infty} dt' K(t') e^{-\alpha_0 t'}$. Using a previously proposed parameterization of $K(t) = N_0 e^{-\alpha_0 t}(1 - A_0(\alpha_0 t + 1/2\alpha_0^2 t^2))$[8] we find that $\kappa = 0.1$ ($A_0 = 0.5$). Thus,

$$k_0(C) \approx \frac{v_r^2}{\alpha_0} \frac{(1 - \kappa\alpha_A(C)/\alpha_0)}{(1 + \alpha_A(C)/\alpha_0)^2} \tag{6}$$

The authors then postulate that

$$\alpha_A(C) = \alpha_0 e^{(C - C_1)/C_0} \tag{7}$$

and empirically determine the contents C_1 and C_0 by fitting the measured dependence of front migration rate on agar concentration. They compute $C_1 = 0.28\%$ and $C_0 = 0.035\%$.

They show that the efficient limit described above captures the dependence of the rate of migration on agar concentration as well as changes in the shape of the front due to changes in agar concentration. Using equations (4), (6) and (7) for our conditions (C = 0.3%) with previously measured values of D_b and k_0 in liquid,[9] we estimate D_b and k_0 in the presence of agar for both rich and minimal medium conditions.

To generate the heat maps shown in Figures 2 and 4 of the main text, we varied $|v_r|$ and k_g. Tumble frequency (α_0) was assumed fixed for these simulations since changes in tumble frequency alone were found to drive only small changes in front migration rate (Figure 2 - figure supplement 3). We therefore recomputed D_b and k_0 for each value of $|v_r|$ and k_g and performed a simulation of front migration.

To estimate how the evolution of run tumble statistics at the single-cell level (Figure 3, main text) in liquid changed D_b and k_0 we assumed $K(t)$ and α_A were unchanged by selection. We recomputed equations (4) and (6) using the observed changes in α_0 and $|v_r|$ (Tables 12 and 13, main text). We then simulated equations 1 and 2 from the main text using these values and the measured change in growth rates (Figure 3(e-f), main text). We found that these changes predicted an increasing rate of migration with selection which was qualitatively correct (Figure 4 - figure supplement 1). We note that our single-cell measurements were made in a uniform environment without spatial gradients in attractants and we therefore cannot determine whether or not K has changed during selection.

V. THE EFFECT OF BOUNDARY INTERACTIONS IN MICROFLUIDIC DEVICE ON RUN-TUMBLE STATISTICS

When *E. coli* swims very close to a surface, interactions between the helical bundle and the surface can result in cells swimming in circles.[10,11] However, wild type cells execute tumbles even in the presence of surfaces[11] and previous methods for tracking single-cells similar to ours have found that cells exhibit typical run-tumble behaviors even in microfluidic devices with a floor to ceiling height as small as 4 µm.[12] Our chambers are 10 µm in depth and we typically observe run-tumble behavior similar to that shown in Figure 3 – figure supplement 1. However, we did transiently observe cells "circling" likely due to close proximity to the floor or ceiling of the chamber. To check that this circling behavior was not biasing our results we devised an automated technique to detect circling. For each run event longer

than 10 frames we compute the sign of $\omega(t)$ for each frame included in the run which we denote $sign(\omega_{run}(t))$. For each run we compute $\xi = |\langle sign(\omega_{run}(t))\rangle|$. ξ is close to unity for cells that are circling and close to zero for cells that are not circling. By inspection of trajectories we determined that cells with $\xi > 0.17$ more than 65 % of the time could be regarded as circling. This classified approximately 15 % of the data as circling due to boundary interactions. The data shown in Figure 3 and all supplemental figures excludes these circling cells. However, we checked that the conclusions of our study, most importantly changes in run speed, were not qualitatively altered even when we included circling cells in our analysis.

VI. COMPARISON OF RICH MEDIUM ROUND 15 STRAIN WITH RP437

We tested whether or not the strain selected for fast migration in rich medium differed substantially from the RP437 strain most commonly used in chemotaxis studies. We measured the migration rate for RP437 to be $0.15\pm0.009\,\mathrm{cm\,h^{-1}}$ in rich medium, approximately a factor two slower than MG1655-motile (founder strain) in identical conditions. We observed similar single-cell behavioral statistics between the two strains (Figure 1 - figure supplement 4) so we attributed slower migration to the reduced growth rate of RP437 relative MG1655-motile ($1.1\pm0.02\,\mathrm{h^{-1}}$ and $1.24\pm0.02\,\mathrm{h^{-1}}$ respectively) measured in well mixed liquid culture.

VII. EXPERIMENTAL DETAILS OF MUTANT RECONSTRUCTION

To reconstruct point mutations in the chromosome of the founding strain, we followed a method described in Kuhlman and Cox[13] and outlined in the Methods section of the main text. Here we detail the experimental methods used in this reconstruction.

A. Preparation and electroporation of electrocompetent cells

0.5 mL of an overnight culture was added to a flask containing 30 mL of LB with appropriate antibiotic(s) and inducer(s) and grown at 30 °C with shaking until the OD600 reached 0.5 to 0.7. The flask was removed and the culture was cooled by swirling in an ice water

slurry for five minutes then placed on ice for ten minutes. The culture was transferred to a pre-chilled centrifuge tube and pelleted by centrifugation (5 min, 5K RPM) in a refrigerated centrifuge chilled to 4 °C. The supernatant was dumped and the cells were washed in 10 mL of ice cold 10 % glycerol. Glycerol wash was repeated twice followed by a resuspension in 200 µL. The cells were immediately placed on ice and kept cold until electroporation. Typically, ~100 µL of cells was mixed with ~5 µL of DNA in a pre-chilled microcentrifuge tube before being transferred to a pre-chilled 0.1 cm gap electroporation cuvette (USA Scientific) and electroporated at 2 kV in an Electroporator 2510 (Eppendorf).

B. Synthesis and integration of the landing pad

Custom primers were designed and ordered from Integrated DNA Technologies. These primers contain homologies to *tetA* flanking regions on template plasmid pTKLP-*tetA* as well as 50bp homologies just upstream/downstream of the desired chromosomal mutation site. PCR using these primerse generated the linear landing pad fragment for each desired mutation site. Purification was performed with AmpureXP magnetic beads followed by a DpnI digest and an additional AmpureXP cleanup. Fragment length was confirmed by 1 % agarose gel. Electrocompetent founder+pTKRED cells were prepared from frozen stock, with IPTG induction of the λ-Red enzymes on pTKRED. These cells were transformed with the landing pad fragment. After 4h outgrowth on the bench, half the culture was pelleted in a microcentrifuge (1min, 14 000 RPM). 410 µL of the supernatant was removed, cells were resuspended in the remaining media and plated on LB+tetracycline+spectinomycin plates. The remaining half of the culture was plated in the same way after an additional day of outgrowth on the bench. The plates were grown at 30 °C and colonies typically took a few days to appear at this step. PCR and 1 % agarose gel electrophoresis on resultant colonies was used to confirm successful landing pad integration at the desired site. The presence of a secondary band consistent with the wild-type revealed heterogeneity within transformant colonies. The landing pad strain was therefore purified by overnight growth (30 °C, shaking) in LB+tetracycline+spectinomycin followed by serial dilution and plating.

C. Integration of desired mutation

A 70bp oligo containing each desired mutation was designed following the design considerations outlined in Sawitzke *et al.*[14] as closely as possible and ordered from Integrated DNA Technologies. Electrocompetent founder+pTKRED+LP cells were prepared from frozen stock, with 2 mM IPTG induction of the λ-Red enzymes as well as 0.4 % w/v L-Arabinose induction of Isce-I from pTKRED. These cells were electroporated with the oligo and 1 mL of LB was immediately added. The cells were then transferred to a flask containing 100 mL of RDM+0.5 % glycerol with inducers and antibiotic. The flask was grown for 2 h at 30 °C with shaking before adding $NiCl_2$.

The appropriate $NiCl_2$ concentration was determined in a separate experiment wherein growth of founder+pTKRED as well as founder+pTKRED+LP, for each landing pad construct, was assayed in the supplemented RDM described above. At each day of the outgrowth until successful transformants were identified, a sample was diluted and plated on LB+spectinomycin. Colonies from these plates were screened for tetracycline resistance. A few tetracycline-susceptible colonies were checked for successful landing pad removal by colony PCR and 1 % agarose gel electrophoresis. Finally the pTKRED plasmid was cured by growth at 42 °C. Mutations were confirmed by Sanger sequencing.

VIII. MODELING EVOLUTION OF CORRELATED TRAITS

The model of evolving correlated traits is derived in detail elsewhere.[15] We infer constraints on entries in the matrix G by comparing the predicted ($\hat{\phi}_{pred}$) direction of phenotypic evolution to that which we observed ($\hat{\phi}_{obs}$). We determined the observed direction of phenotypic evolution by linear regression of the data shown in Figure 4(a) of the main text. We then compute the dot product $\hat{\phi}_{pred} \cdot \hat{\phi}_{obs}$ over a range of values of $\sigma_{\tilde{k}_g}$, $\sigma_{|\tilde{v}_r|}$ and ρ (Figure 6 – figure supplement 2).

We note that the migration rate in minimal media as a function of $|v_r|$ and k_g contains a strong nonlinearity around a growth rate of $0.2\,\mathrm{h}^{-1}$. This transition occurs between regimes where bacterial transport is dominated by growth and diffusion (founder) and chemotaxis (evolved).[5] The characteristic timescale for the migration process is set by the growth rate $\tau \sim 1/k_g$ and the length scale by the distance a cell diffuses over its lifetime $l \sim \sqrt{D_b/k_g}$.

For the founding strain in minimal medium, τ ~10 h while $l \sim 0.5$ cm. In this case ∇c remains small and transport is dominated by diffusion and subsequent growth. As growth rates increase during selection and D_b decreases only modestly (see Table 13, main text) and τ ~3 h and $l \sim 0.15$ cm. In this case chemotactic transport becomes substantial due to gradients that form over lengthscale l and we observe this transition to traveling waves around k_g ~0.2 h^{-1}. We note that this transition predicted by our model is also observed experimentally (Figure 1(e), main text).

However, as a result of this non-linearity our estimate of $\vec{\beta}$ in minimal medium relies on a poor linear fit (Figure 6 – figure supplement 1). To asses whether or not this poor approximation might alter our conclusions we performed stochastic simulations of an evolving population that did not require us to make a linear approximation to infer $\vec{\beta}$. To accomplish this we generated a population of 1000 individuals whose phenotype was drawn from the multivariate normal distribution $\mathcal{N}(\vec{\phi}^f, G)$ where $\vec{\phi}^f$ is the mean phenotype of the founding population and G is the genetic covariance matrix discussed in the main text. Using the predicted migration rate as a function of $|v_r|$ and k_g as a fitness landscape (Figure 2(b), main text) we then select that fastest 1 % of the population. From this selected population we compute a new $\vec{\phi}^1$ and generate a second population from the distribution $\mathcal{N}(\vec{\phi}^1, G)$. The process is repeated iteratively. The results of these simulations are shown in Figure 6 - figure supplement 3. We find that our qualitative conclusions hold. Large negative values of the train correlation coefficient ($\rho < -0.9$) and $\sigma_{\tilde{k}_g} > \sigma_{|\tilde{v}_r|}$ result in evolution in the same direction we observe experimentally. We note that in these simulations populations with finite $\sigma_{|\tilde{v}_r|}$ and $\rho > -1$ are able to evolve both higher run speeds and growth rate.

IX. ESTIMATED CHANGE IN DRAG DUE TO CHANGE IN GROWTH RATE

For a bacterium swimming at constant speed u (at low Reynolds number) the propulsion force provided by the flagella equals the drag force from the fluid. Thus, we can write:

$$u = \frac{F_{flag}}{F_D/u} \tag{8}$$

The ratio of swimming speeds in a given medium for evolved and founding strains is therefore:

$$\frac{u^{ev}}{u^f} = \frac{F^{ev}_{flag}\left(F^{ev}_D/u^{ev}\right)^{-1}}{F^{f}_{flag}\left(F^{f}_D/u^{f}\right)^{-1}} \tag{9}$$

If we assume the flagellar force is unchanged with selection, then we have:

$$\frac{u^{ev}}{u^f} = \frac{F_D^f/u^f}{F_D^{ev}/u^{ev}} \tag{10}$$

The drag force on an ellipsoid moving along its symmetry axis at speed u in a fluid with viscosity μ is given by equation (2.3) in R.G. Cox:[16]

$$F_D = 16\pi\mu a u \left[\frac{-2\chi}{\chi^2-1} + \frac{2\chi^2-1}{(\chi^2-1)^{\frac{3}{2}}} + \ln\frac{\chi+\sqrt{\chi^2-1}}{\chi-\sqrt{\chi^2-1}}\right]^{-1} \tag{11}$$

Where χ is the ratio of the major axis (half-length) b to the minor axis (half-width) a.

$$\chi = \frac{b}{a} = \frac{l/2}{w/2} = \frac{l}{w} \tag{12}$$

It can be shown that (11) is equivalent to:

$$F_D = 6\pi\mu a u K' \tag{13}$$

where

$$K' = \frac{\frac{4}{3}(\chi^2-1)}{\frac{2\chi^2-1}{\sqrt{\chi^2-1}}\ln\left[\chi+\sqrt{\chi^2-1}\right]-\chi} \tag{14}$$

Using the above, we have:

$$\frac{u^{ev}}{u^f} = \frac{w_f K'_f}{w_{ev} K'_{ev}} \tag{15}$$

Taheri-Araghi *et. al*[17] figure S1(A) gives the average length and width of an *E. coli* as a function of its growth rate:

$$l = 2.08 * 2^{0.41*\frac{divisions}{hour}}\mu m = 2.08 * 2^{0.41*\frac{r}{\ln 2}}\mu m \tag{16}$$

$$w = 0.41 * 2^{0.36*\frac{divisions}{hour}}\mu m = 0.41 * 2^{0.36*\frac{r}{\ln 2}}\mu m \tag{17}$$

Using this expression for the width, we have:

$$\frac{u^{ev}}{u^f} = \frac{K'_f}{K'_{ev}} * 2^{0.519(r_f - r_{ev})} \tag{18}$$

From our growth rate experiments, we have:

r^f_{LB} =1.24 h^{-1} r^f_{gal} =0.08 h^{-1}

r^{ev}_{LB} =1.09 h^{-1} r^{ev}_{gal} =0.40 h^{-1}

Using these values, we can calculate χ (and therefore K') from equations (16) and (17) and plug these into (18). Doing this, we find that:

$$\frac{u_{LB}^{ev}}{u_{LB}^{founder}} = 1.059$$

$$\frac{u_{gal}^{ev}}{u_{gal}^{founder}} = 0.884$$

We see that the change in drag due to the change in cell size that we calculate using (16),(17) and our growth rate data would only account for a 6% swimming speed increase in LB and a 12% swimming speed decrease in galactose. We note that the growth rates of our strains in rich medium (LB) lie within the range of growth rates measured by Taheri-Araghi *et. al*, however the growth rates in galactose minimal medium are significantly slower. Finally, since we have not measured cell size in our evolved strains we cannot definitively rule changes in size as a mechanism for the trade-off observed here.

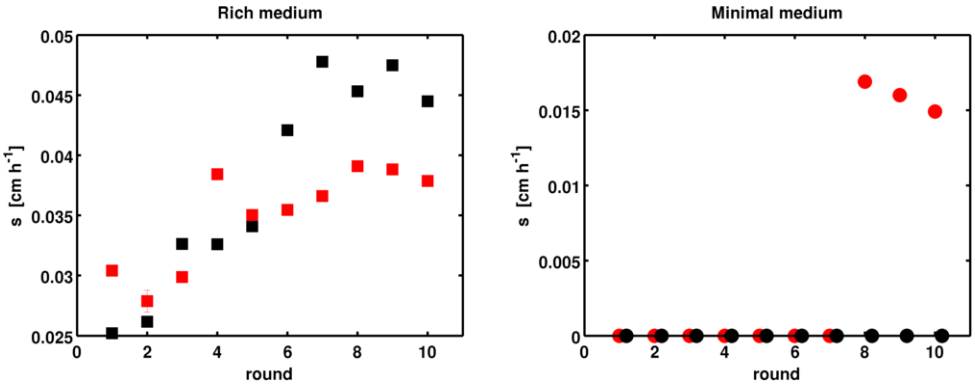

Figure 1 - figure supplement 1. Selection with non-chemotactic (ΔcheA-Z) mutant: Front migration rates of non-chemotactic mutants in 0.3 % w/v agar at 30 °C with LB (left panel) and M63 0.18mM galactose (right panel). Errors are smaller than the size of the markers, except for the red replicate in rich medium at round 2. Red and black correspond to two independent selection experiments. Note the vertical scales. In minimal medium zero migration rate denotes plates where density increased in the vicinity of the site of inoculation but no migration was observed. In these cases no measurable migration rate was obtained.

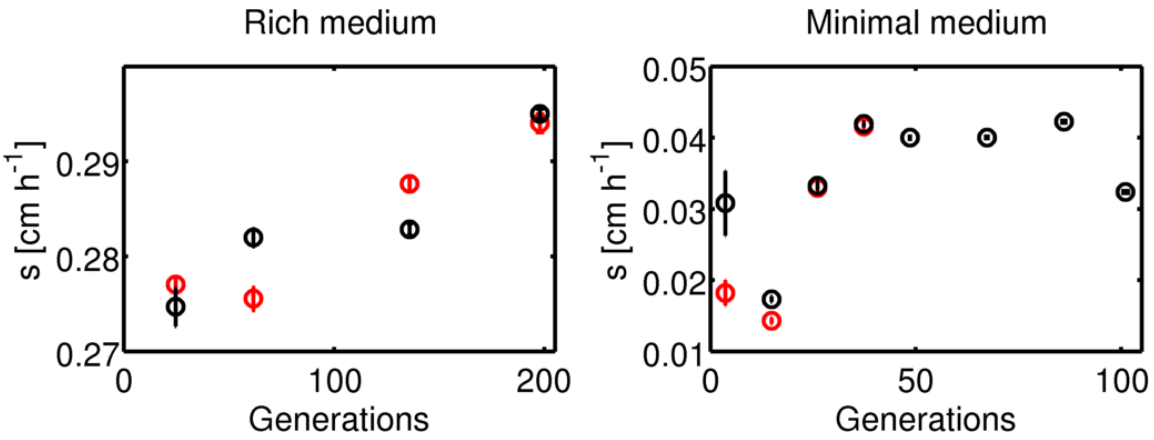

Figure 1 - figure supplement 2. Change in migration rate during long-term liquid culture: (left) The founder strain (Figure 1, main text, $s = 0.3 \pm 0.01\,\mathrm{cm\,h^{-1}}$) was inoculated into a turbidostat and continuously cultured in LB at 30 °C for approximately 200 generations. Samples were periodically drawn from the turbidostat and used to inoculate 0.3 % w/v agar LB plates. Migration was recorded via webcam as as described in the main text. Error bars are standard errors from regression of radius with time. Note the scale on the y-axis. (right) Identical experiment in minimal medium conditions. Founding strain was grown in a single chemostat (doubling time 6.4 h) in minimal medium for 100 generations. Plates were inoculated from samples drawn from the chemostat, two plates at each time point for the first four time points and then one plate at each time point. The last four time points (where the rate appears to saturate) exhibit a slower migration rate than the round 10 migration rates in Figure 1(e) ($p = 0.02$).

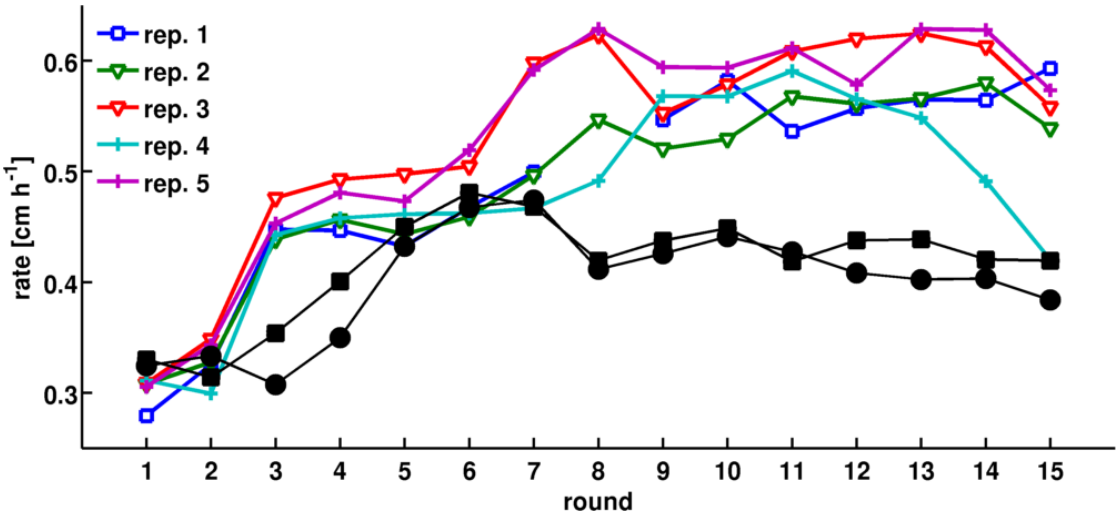

Figure 1 - figure supplement 3. Adaptation in rich medium depends on sampling location: Migration rate as a function of the round of selection. Colored traces are reproduced from Figure 1 in the main text. Black circles and squares are two replicate selection experiments where populations are sampled halfway between the center of the colony and the outer edge after each round of selection.

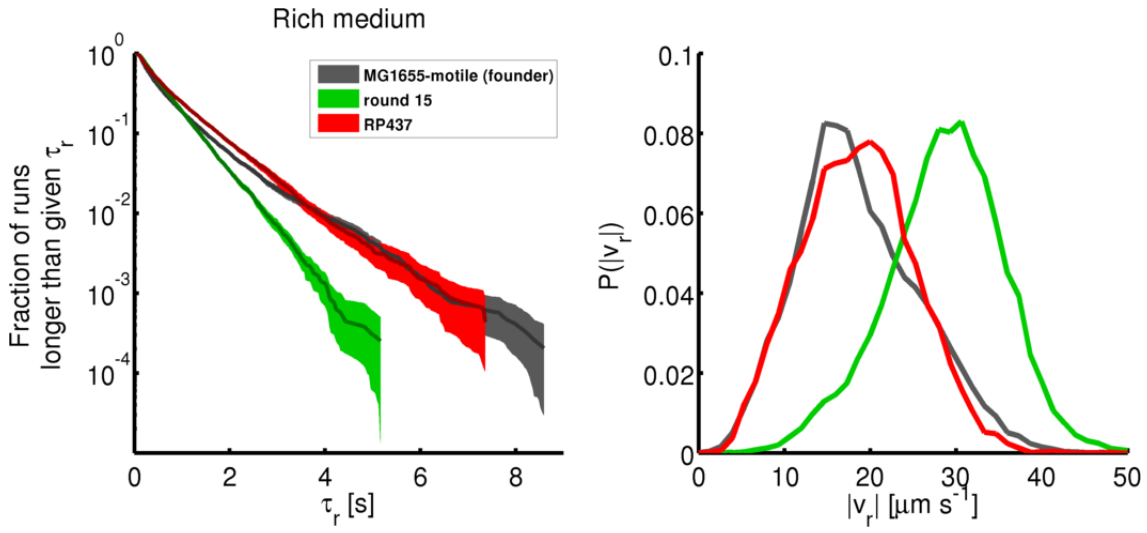

Figure 1 - figure supplement 4. Comparison of founding and evolved strains to RP437: Single-cell swimming in rich medium: (left) Run duration distributions identical to those shown in Figure 3(a-b) of the main text. 77 RP437 individuals were tracked from a culture at the same optical density as founder and round 15 (replicate 1). A total of 9218 run events were recorded. The average ± standard deviation in run duration for RP437 is 0.76±0.82 s. (right) Comparison of run speeds for the same three strains. RP437 has an average ± standard deviation in run speed of 18.58±6.4 µm s^{-1}. The average run duration for RP437 exceeds that of round 15 ($p < 10^{-4}$ and the average run speed is smaller than that of round 15 ($p < 10^{-4}$).

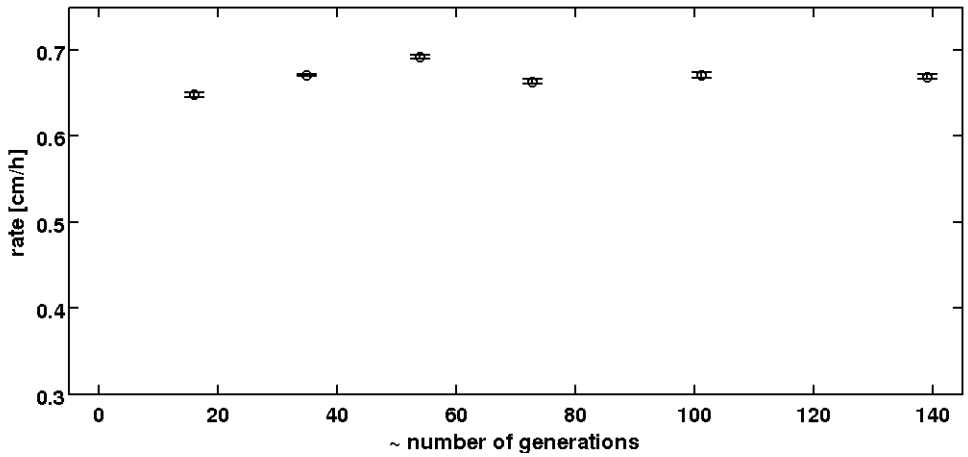

Figure 1 - figure supplement 5. Round 15 Persistence of rich medium fast migrating phenotype in rich medium: A strain isolated after 15 rounds of selection in rich medium (Figure 1(c), replicate 1, main text, $s = 0.6\,\mathrm{cm\,h^{-1}}$) was inoculated into a turbidostat and continuously cultured in LB at 30 °C for approximately 140 generations. The number of generations was estimated assuming a constant generation time of 36 min. Samples were periodically drawn from the turbidostat and used to inoculate 0.3 % w/v agar LB plates. Migration was recorded via webcam as as described in the main text. Error bars are standard errors from regression of radius with time.

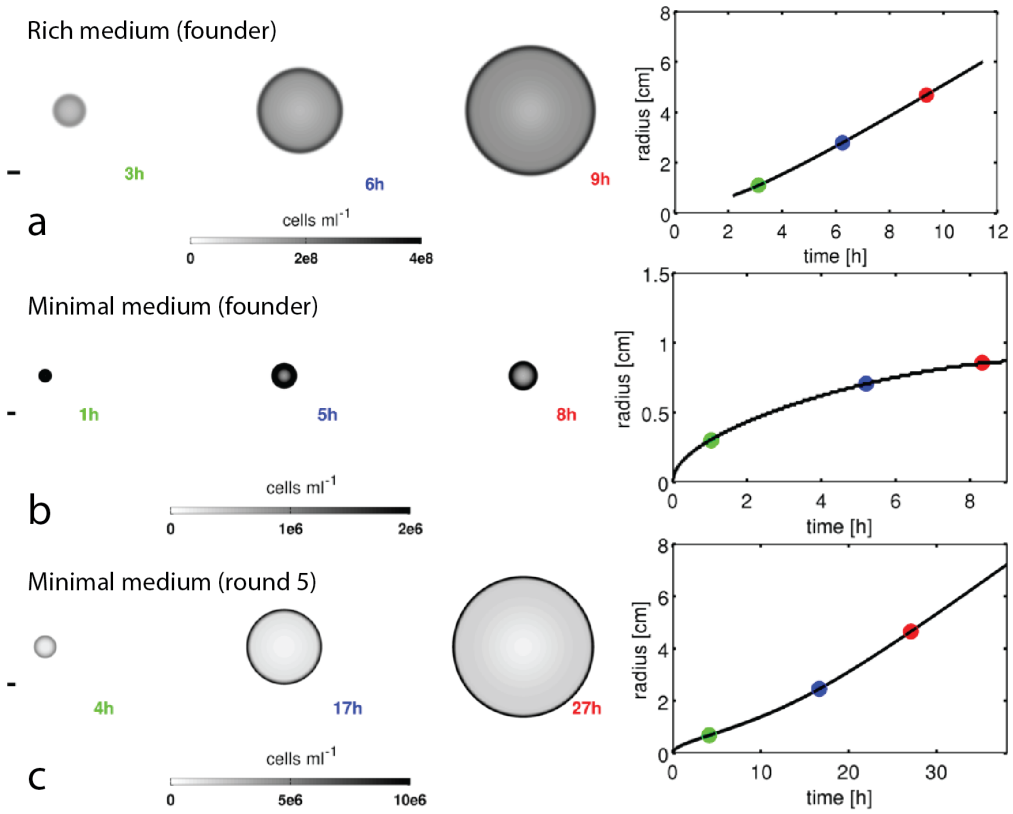

Figure 2 - figure supplement 1. Reaction-diffusion model recapitulates qualitative features of colony expansion: Results from numerical simulations of the reaction-diffusion model in the main text. Simulations for founding strain in rich medium (a), founding strain in minimal medium (b), and round 5 strain in minimal medium (c) are shown. Three snapshots of $\rho(\mathbf{r}, t)$ for each simulation are shown as greyscale heatmaps (note independent color maps). The panel on the right in (a-c) shows the location of the front in time (black trace) and the time points corresponding to the three snapshots are labeled by the colored points. The parameters for each simulation are given in Table 10 and 11 of the main text. The founding strain in minimal medium exhibits diffusive transport due to slow growth, this is also observed experimentally (Figure 1, main text).

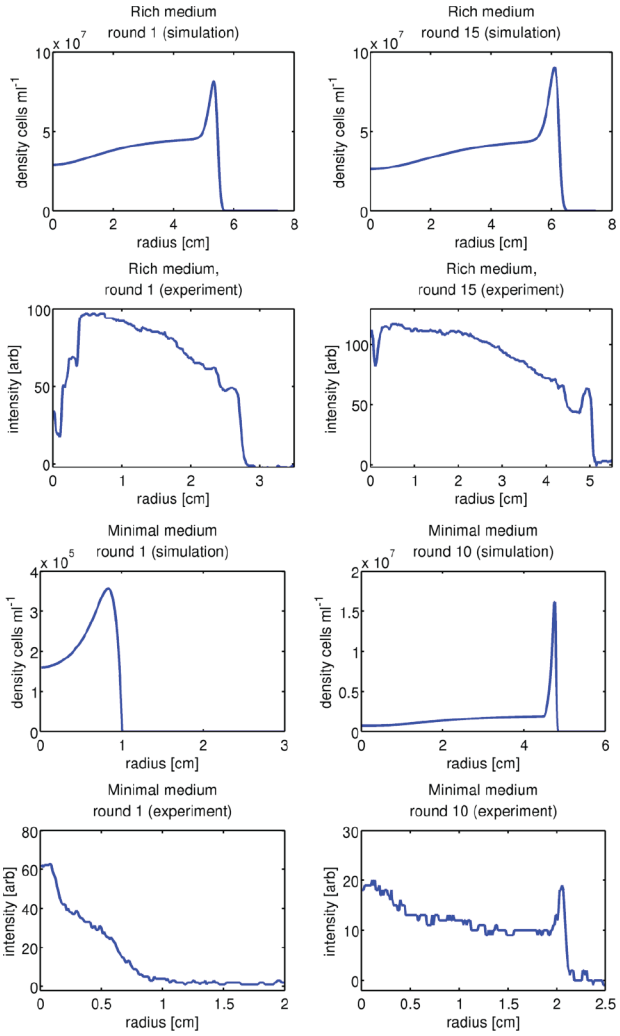

Figure 2 - figure supplement 2. Comparison of front profiles from simulation and experiment: Upper four panels show front density profiles from simulation and experiment for the rich medium condition. Left column shows round 1 and right column round 10. Simulation profiles are taken from time points after a constant rate of expansion has been attained. Experimental front profiles are taken at the end of colony expansion (12 hours). In the experimental front profiles the high density regions arise from metabolism of amino acids other than serine. The lower four panels are identical to the upper four but are taken from minimal medium simulations and experiments.

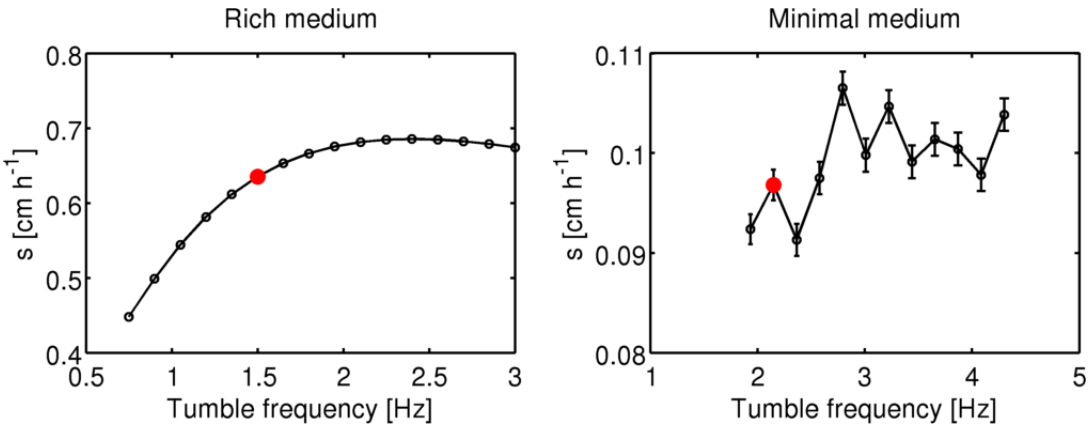

Figure 2 - figure supplement 3. Simulation of migration rate versus tumble frequency: Using the formalism of Croze *et al.* migration rate as a function of tumble frequency (Section IV) was computed using the reaction-diffusion model presented in the main text. Panels show migration rate (s) as a function of tumble frequency (α_0) for rich medium and minimal medium conditions. Red dots indicate measured tumble frequency in each condition (Figure 3, main text). Error bars in the left panel are smaller than the size of the markers. Error bars in the right panel are standard errors from a linear regression on the front location in time. The non-monotonic variation of migration rate with tumble frequency in minimal medium results from the slight curvature in the front location as a function of time in these conditions (see Figure 2 - figure supplement 1 (right panel)).

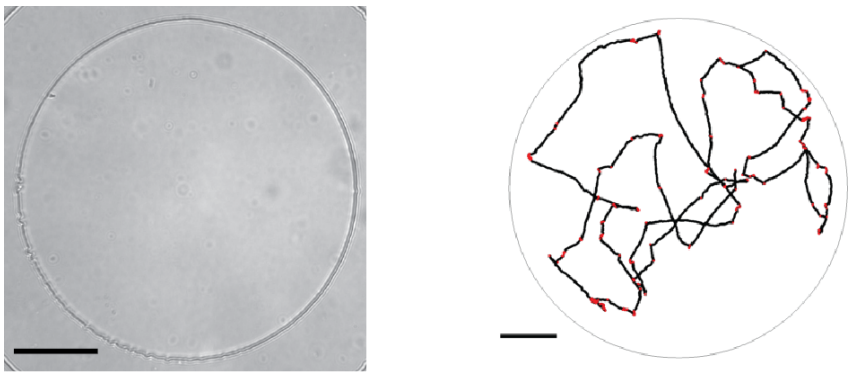

Figure 3 - figure supplement 1. Microfluidic device and single-cell swimming trajectory: (left) Bright-field image at 20× magnification of the PDMS microfluidic chamber used to trap single bacteria. The boundary of the chamber can be seen as the high contrast circle. Scale bar is 50 µm. (right) A segmented trajectory of a single cell in a chamber like the one shown on the left. Dots indicate locations of the centroid. Black portions indicate running events and red portions tumbles. Image processing and run-tumble detection are described in the Methods section of the main text.

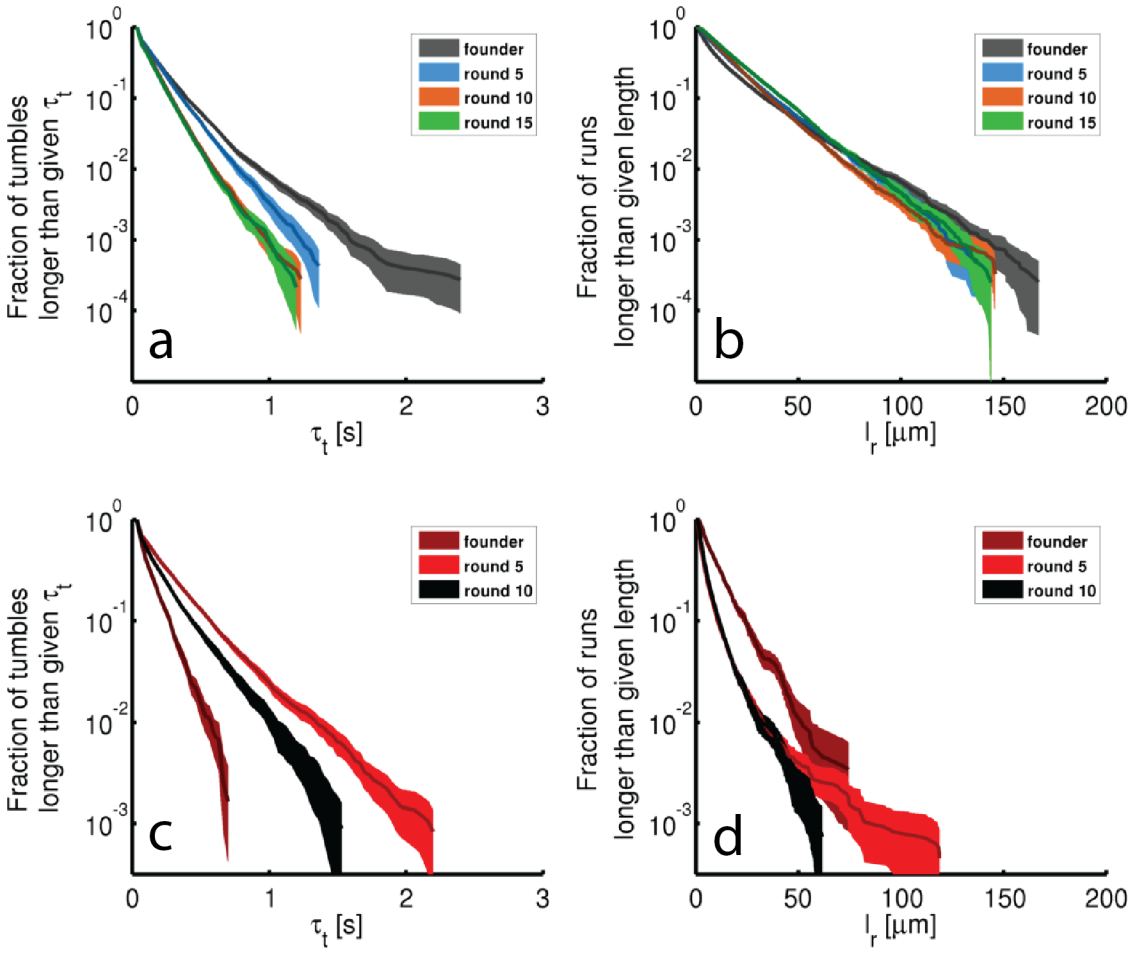

Figure 3 - figure supplement 2. Tumble durations and run lengths for evolved strains: Tumble durations (τ_t) and run lengths (l) for single-cell tracking shown in Figure 3 of the main text. (a) shows the complementary cumulative distribution of tumble durations for rich media evolved strains. Shaded regions are 95 % confidence intervals from bootstrapping. Averages and standard deviations are: 0.18±0.2 s, 0.17±0.16 s, 0.14±0.13 s, 0.14±0.12 s for founder, round 5, 10 and 15 respectively. (b) Identical to (a) except constructed for run lengths. The run length is found by computing the arc-length between tumble events for each run. The averages and standard deviations are 13.5±17.7 µm, 16.5±17.4 µm, 16.5±16 µm, 19±17.8 µm respectively. (c) and (d) are identical to (a) and (b) for minimal medium evolved strains (replicate 1). The tumble durations are 0.13±0.11 s, 0.25±0.27 s, 0.19±0.21 s for founder, round 5 and 10. The respective run lengths are 11±11.6 µm, 5±7.5 µm and 5.3±6.6 µm.

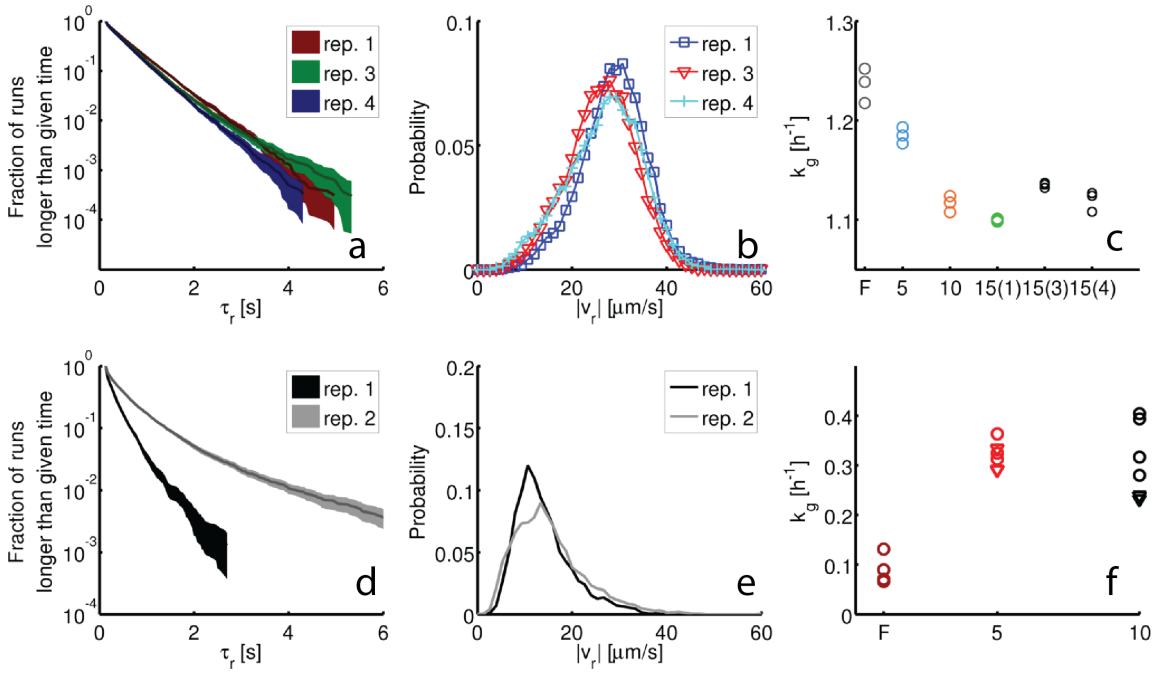
Fraction of runs longer than given time
rep. 1
rep. 3
rep. 4
a
τr [s]
Probability
b
|vr| [µm/s]
kg [h-1]
c
F 5 10 15(1)15(3)15(4)
rep. 1
rep. 2
d
e
f

Figure 3 - figure supplement 3. Reproducibility of the evolved phenotype: Single-cell tracking and growth rate measurements were performed on independently selected strains in rich medium (15 rounds, (a-c)) and minimal medium (10 rounds, (d-f)). Panels show run durations (a,d), run speeds (b,e) and growth rates (c,f). Single-cell tracking experiments were performed on two additional round 15 strains from the rich medium experiment (replicates 3 and 4, Figure 1(c) main text). For replicates 1, 3 and 4 - 96, 85 and 98 individuals were tracked for a total of 15 928, 16 639 and 18 171 run events respectively. (a) shows the run duration distributions for these three strains with mean± standard deviations: 0.65±0.57 s, 0.60±0.53 s, 0.57±0.49 s respectively. (b) Run speed ($|v_r|$) distributions for the same three strains with means 28.7 µm s^{-1}, 26.2 µm s^{-1} and 26.7 µm s^{-1} respectively. (c) maximum growth rates (k_g) for the same two independently evolved strains (with 15(3) denoting replicate 3 and 15(4) denoting replicate 4). The decline in growth rate relative to founder is significant for both replicate 3 ($p < 10^{-3}$) and replicate 4 ($p < 10^{-3}$) (d-f) show swimming statistics and growth rates for independently evolved strains in minimal medium, replicate 1 and 2 correspond to Figure 1(e) in the main text. (d) Run duration distributions for constructed for 29 individuals from replicate 1 and 80 individuals from replicate 2 corresponding to 5384 and 9357 run events respectively. The with mean± standard deviations are: 0.34±0.30 s and 0.65±0.87 s. (e) Run speed distributions for independently evolved minimal medium strains. Means for replicates 1 and 2 are 13.9 µm s^{-1} and 15.25 µm s^{-1} respectively. (f) Growth rates for founder, rounds 5 and 10 reproduced from Figure 1(e), main text (circles) along with growth rate measurements for strain isolated from round 5 of replicate 2 (red triangles) and round 10 of replicate 2 (black triangles). Means are 0.3 h^{-1} and 0.24 h^{-1}. Round 5 growth rates do not differ significantly ($p = 0.24$) while round 10 growth rates do ($p = 0.02$). Both replicate 2 strains from rounds 5 and 10 exhibit growth rates are larger than founder ($p < 0.001$).

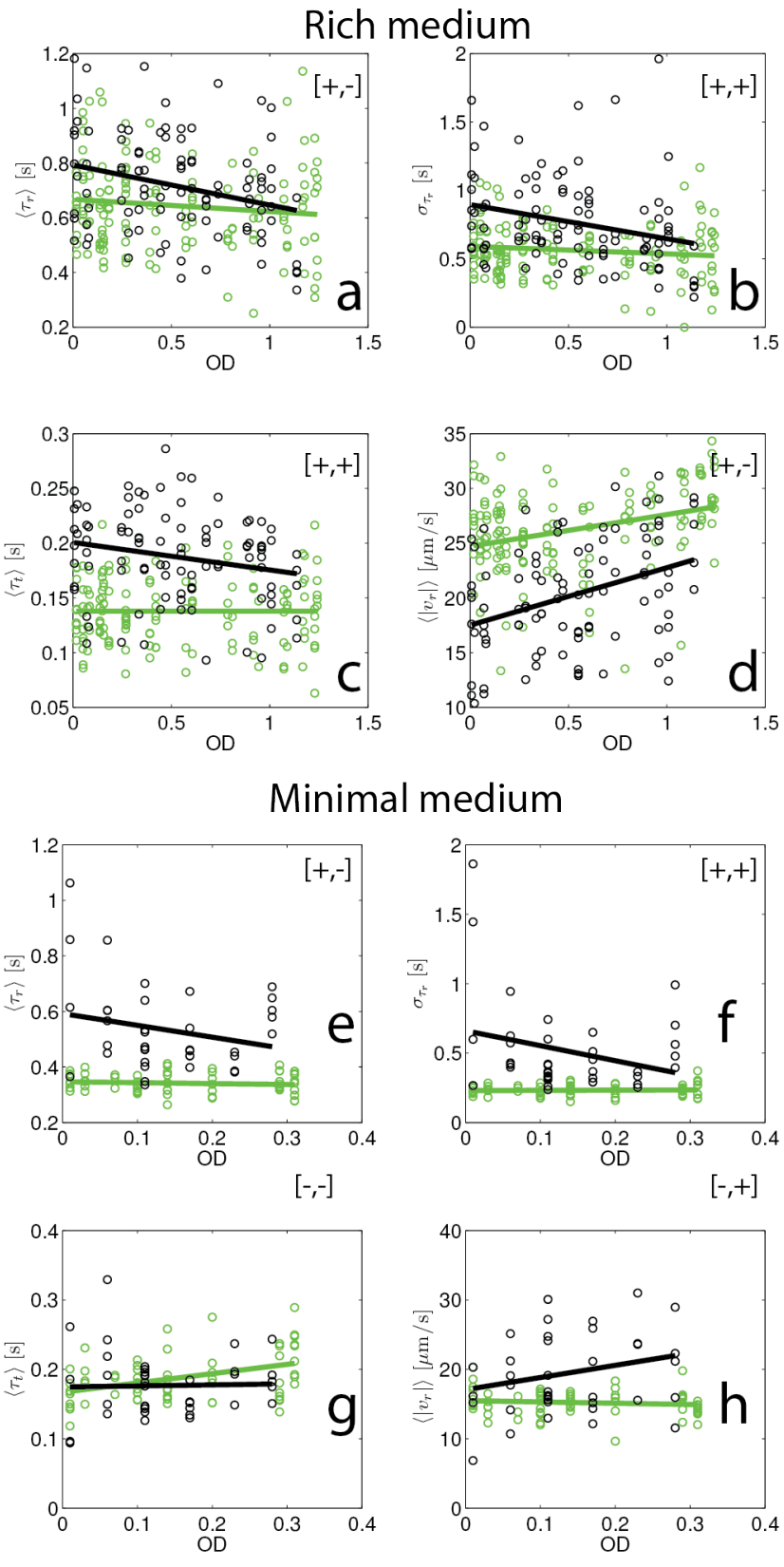
Rich medium
[+,-]
[+,+]
[+,+]
[+,-]
a
b
c
d
OD
$\langle \tau_r \rangle$ [s]
σ_{τ_r} [s]
$\langle \tau_t \rangle$ [s]
$\langle |v_r| \rangle$ [μm/s]
Minimal medium
[+,-]
[+,+]
[-,-]
[-,+]
e
f
g
h
OD
$\langle \tau_r \rangle$ [s]
σ_{τ_r} [s]
$\langle \tau_t \rangle$ [s]
$\langle |v_r| \rangle$ [μm/s]

(preceding page): **Figure 3 – figure supplement 4: Swimming statistics as a function of culture density:**(a-d) Show swimming statistics (τ_r, σ_{τ_r}, τ_t and $|v_r|$) as a function of culture optical density for rich medium founding (green) and evolved (black, round 15, replicate 1). Each point corresponds to a single individual tracked for up to 5 minutes. 141 individuals were tracked from founder (black) and 96 individuals were tracked from round 15. Solid lines are linear regressions. (e-h) Show identical plots for minimal medium founding (green) strain and evolved (black, round 10 replicate 1). For all panels the + and – symbols in the brackets in the upper right indicate statistical significance at the 0.05 level for a difference between founder and evolved in [intercept, slope] of the linear regressions shown (F-test).

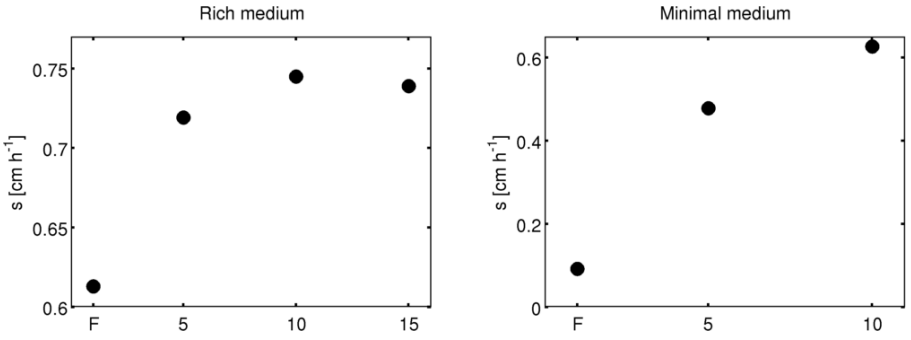

Figure 4 - figure supplement 1. Predicted migration rates for evolved strains: Using the reaction-diffusion model (Main text) we simulated colony expansion using the parameters shown in Tables 10 and 11 of the main text.

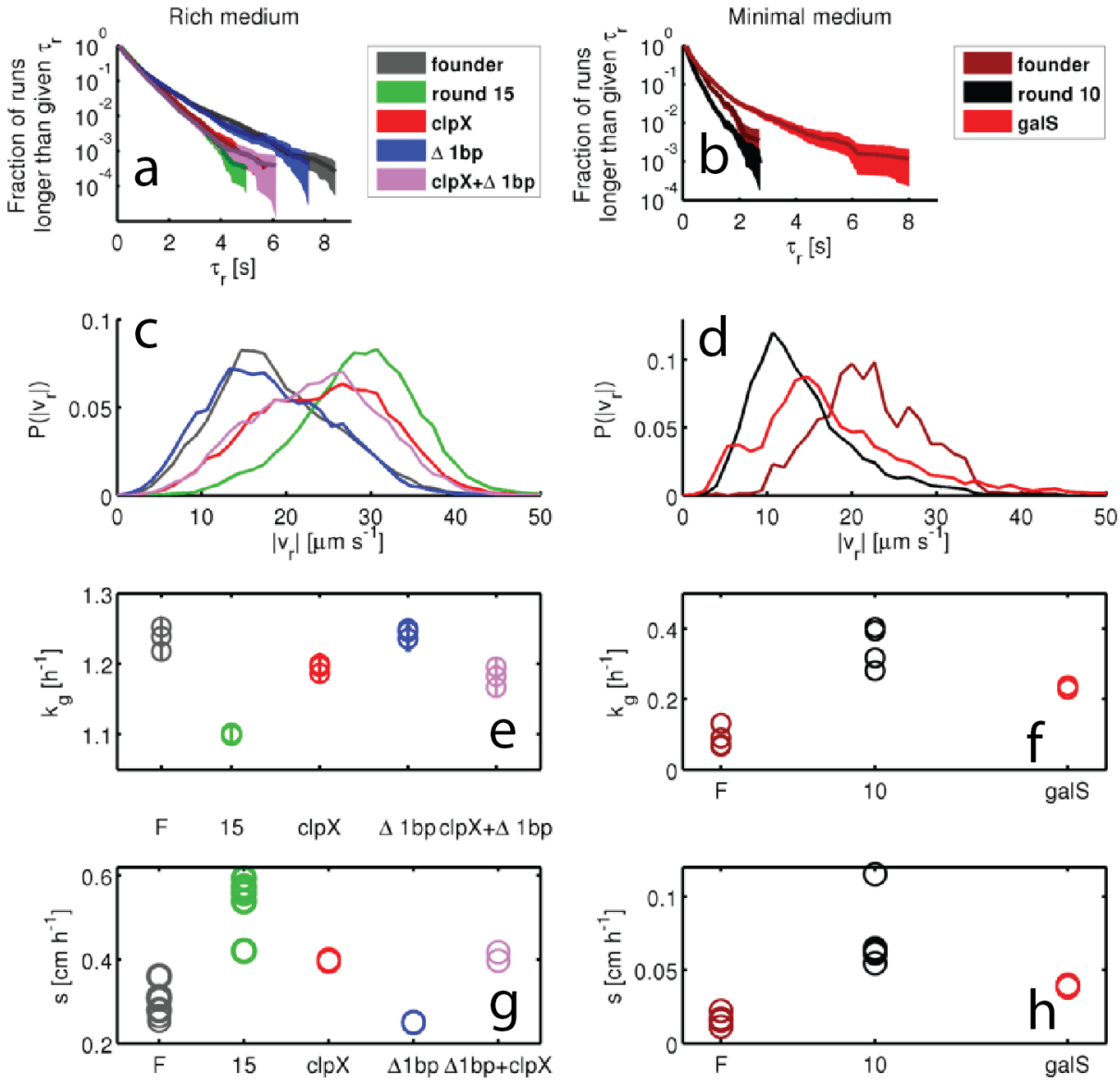
Rich medium
Minimal medium
Fraction of runs longer than given τ_r
τ_r [s]
founder
round 15
clpX
Δ 1bp
clpX+Δ 1bp
round 10
galS
a
b
c
d
e
f
g
h
$P(|v_r|)$
$|v_r|$ [μm s^{-1}]
k_g [h^{-1}]
s [cm h^{-1}]
F
15
clpX
Δ 1bp
clpX+Δ 1bp
10
galS
Δ1bp
Δ1bp+clpX

(preceding page): **Figure 4 – figure supplement 2: Swimming statistics, growth rates and migration rates for mutants:** Run durations (τ_r) and speeds ($|v_r|$), growth rates (k_g) and migration rates (s) for four mutations reconstructed in the founder background (see Main Text). Three mutants were studied in rich medium (a,c,e,g) - *clpX*E185*, a single base pair deletion at position 523 086 (Δ1bp) and the double mutant, (*clpX*+Δ 1bp). One mutant was studied in minimal medium: *galS*L22R. In all panels phenotypes of mutants are compared to founder and the population isolated after the final round of selection in the appropriate environment. (a) shows $c(\tau_r)$ in rich medium, means a standard deviations are: 0.63±0.6 s, 0.66±0.91 s and 0.59±0.55 s for *clpX*, Δ1bp and *clpX*+Δ1bp respectively. *clpX* and *clpX*+Δ1bp have shorter average run durations than founder ($p < 10^{-4}$) (b) $c(\tau_r)$ in minimal medium where *galS*L22R exhibits longer runs than founder with 0.55±0.75 s ($p < 10^{-5}$). (c) gives $P(|v_r|)$ in rich medium. Means ± standard deviations are 24.2±7.8 µm s^{-1}, 18.2±7.3 µm s^{-1} and 23.4±7.6 µm s^{-1} for *clpX*, Δ1bp and *clpX*+Δ1bp respectively. All mutants except Δ1bp exhibit faster runs on average ($p < 10^{-5}$). (d) $P(|v_r|)$ in minimal medium where *galS*L22R has a mean of 17.6±8.7 µm s^{-1} which is lower than founder $p < 10^{-5}$. (e) Growth rates for rich medium mutants. *clpX* and *clpX*+Δ1bp have lower growth rates than founder ($p = 0.0087$ and $p = 0.0069$). The Δ1bp mutation alone does not have a statistically significant difference in growth rate from founder ($p = 0.53$). (f) shows growth rate for the *galS* mutant relative to founder and round 10. the mutant growth rate is larger than founder ($p < 0.001$). (g) shows colony migration rates for mutants in rich medium. *clpX* and *clpX*+Δ1bp differ significantly from the migration rate of founder ($p = 0.0021$ and $p = 0.0017$). Δ1bp does not have a statistically significant change in growth rate. Comparisons are made between duplicate measurements for each genotype and the migration rates of all five replicate experiments in Figure 1 of the main text. (f) Shows migration rate measurements for the *galS* mutant in minimal medium compared to founder and round 10 in minimal medium. The mutant is faster than the founding strain ($p < 10^{-3}$).

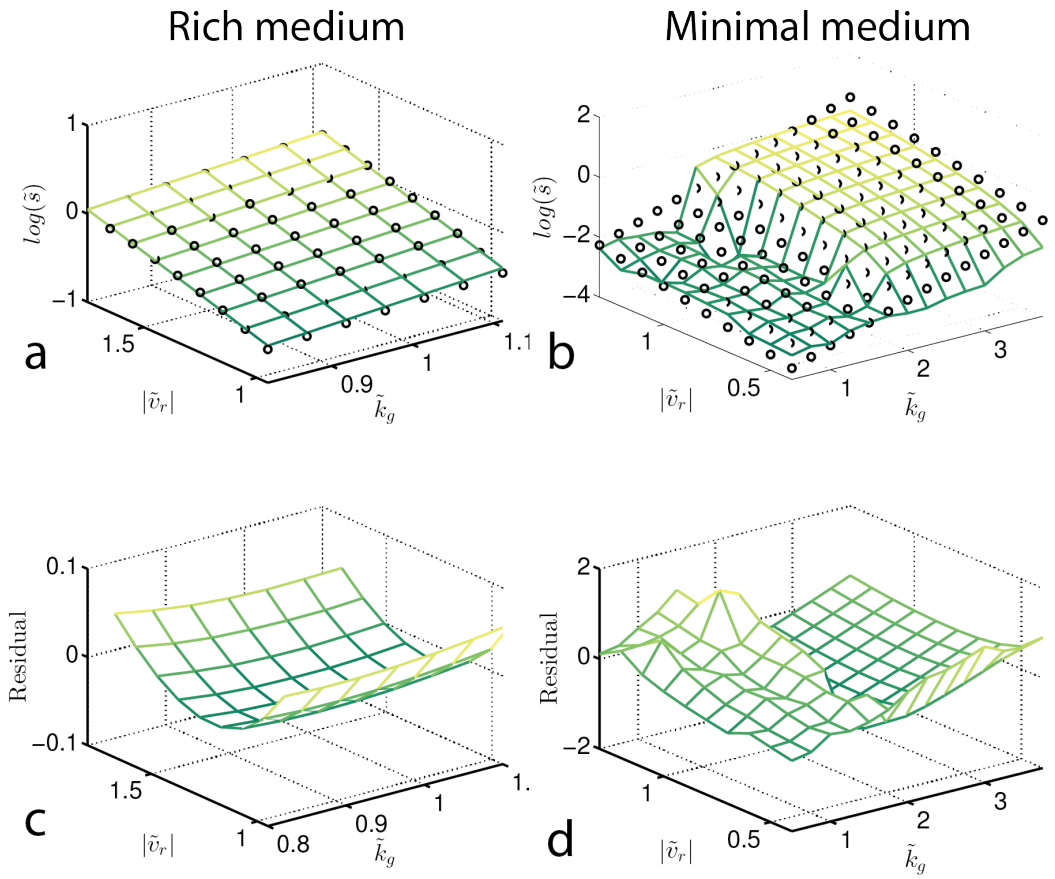

Figure 6 - figure supplement 1. Determining $\vec{\beta}$ from reaction-diffusion model: Reaction-diffusion model was used to simulated migration rates. Panels (a) and (b) plot the normalized (to the founder), predicted, migration rate ($\tilde{s}$) for both rich medium (a) and minimal medium (b). (a-b) are surface plots of the heatmaps shown in Figures 2 and 4 of the main text. To infer the selection pressure $\vec{\beta}$ we fit a plane (black circles) to the surfaces shown in (a) and (b). The residuals of this fit are shown in (c) and (d) respectively. The fit for rich media is good, while the residual is large in minimal medium.

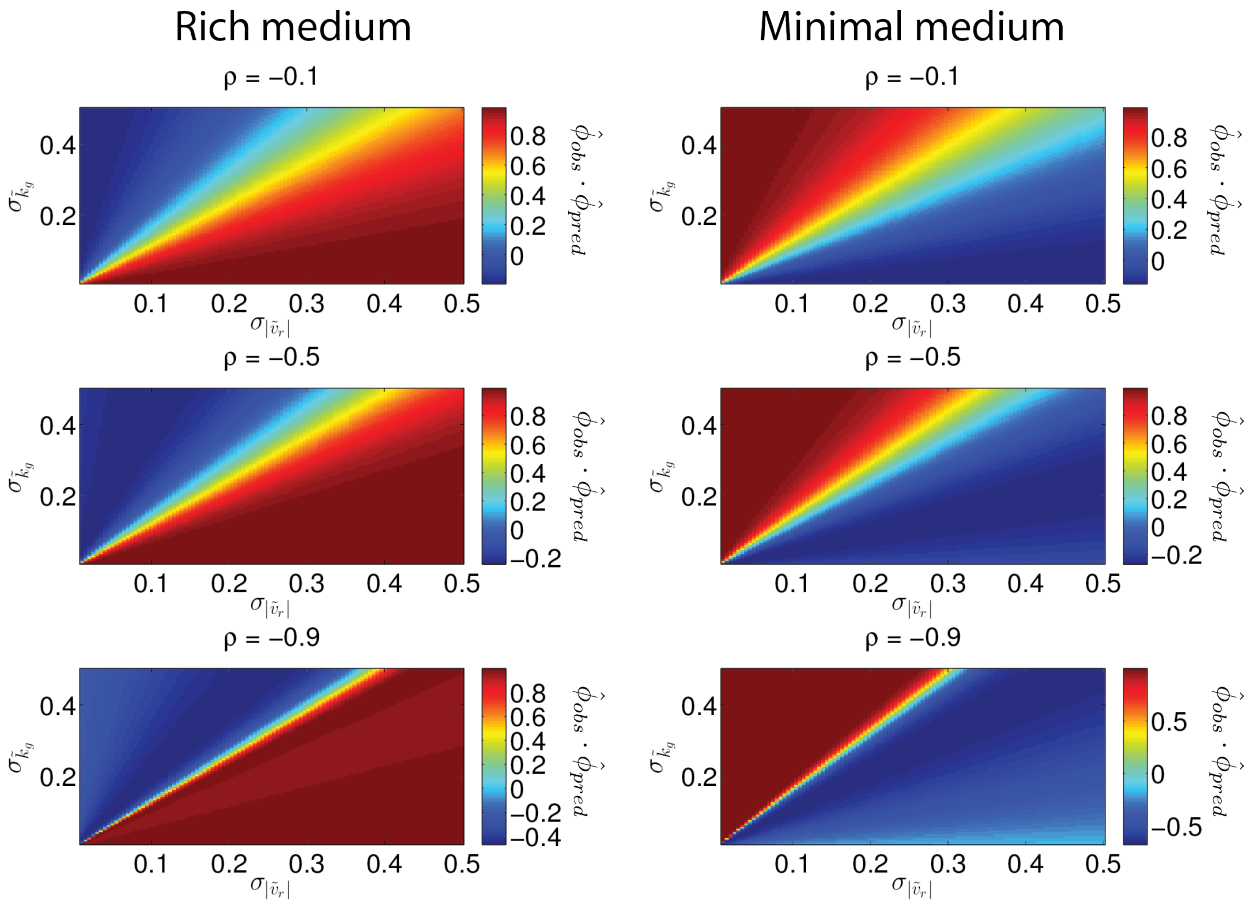

Figure 6 - figure supplement 2. Direction of phenotypic evolution with $\sigma_{|\tilde{v}_r|}$ and $\sigma_{\tilde{k}_g}$: The dot product $\hat{\phi}_{obs} \cdot \hat{\phi}_{pred}$ is plotted as a heatmap as a function of genetic variances in growth rate and run speed. Each row corresponds to a different value of the correlation coefficient (ρ) between run speed and growth rate as labeled. The left column is for rich medium and the right column for minimal medium. When $\hat{\phi}_{obs} \cdot \hat{\phi}_{pred} \to 1$ (dark red) this indicates regions where the predicted direction of evolution ($\hat{\phi}_{pred}$) coincides with the observed direction of evolution ($\hat{\phi}_{obs}$). Note our qualitative conclusions are robust to large variation in ρ.

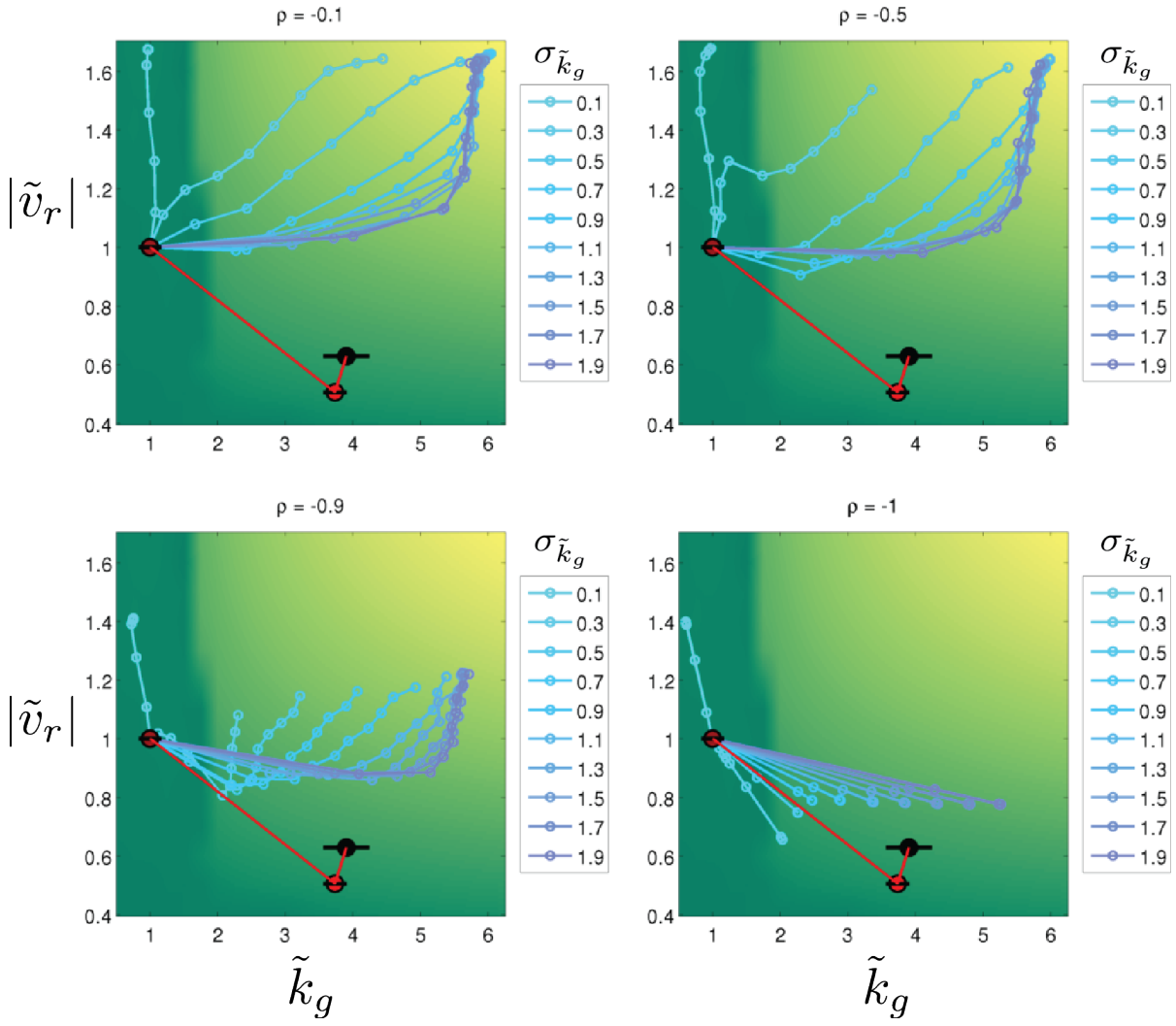

Figure 6 - figure supplement 3. Stochastic simulations of selection in minimal medium: Stochastic simulations of phenotypic evolution in minimal medium. Simulations were carried out as described above. For all simulations $\sigma_{|\tilde{v}_r|} = 0.1$. Each colored line represents a single simulation which initiates at $[1, 1]$. Each point is the mean phenotype for a round of selection. Colors represent different values of $\sigma_{\tilde{k}_g}$ as shown in the legends. The green-yellow heatmap is the "fitness landscape" interpolated from the heatmap shown in Figure 2(b) of the main text. Each panel shows a simulation for different, fixed, values of the trait correlation coefficient ρ. The red line and circles show the observed phenotypic evolution in minimal medium (Figure 4(a), main text).

[1] N. W. Frankel, W. Pontius, Y. S. Dufour, J. Long, L. Hernandez-Nunez, and T. Emonet, eLife **3**, e03526 (2014).

[2] L. Løvdok, M. Kollmann, and V. Sourjik, Journal of biotechnology **129**, 173 (2007).

[3] J. Merritt and S. Kuehn, Scientific Reports **6**, 33173 (2016).

[4] M. A. Rivero, R. T. Tranquillo, H. M. Buettner, and D. A. Lauffenburger, Chemical engineering science **44**, 2881 (1989).

[5] O. A. Croze, G. P. Ferguson, M. E. Cates, and W. C. K. Poon, Biophysical Journal **101**, 525 (2011).

[6] A. Celani and M. Vergassola, Proceedings of the National Academy of Sciences **107**, 1391 (2010).

[7] J. E. Segall, S. M. Block, and H. C. Berg, Proceedings of the National Academy of Sciences of the United States of America **83**, 8987 (1986).

[8] D. A. Clark and L. C. Grant, Proceedings of the National Academy of Sciences of the United States of America **102**, 9150 (2005).

[9] T. Ahmed and R. Stocker, Biophysical Journal **95**, 4481 (2008).

[10] W. R. Diluzio, L. Turner, M. Mayer, P. Garstecki, D. B. Weibel, H. C. Berg, and G. M. Whitesides, Nature **435**, 1271 (2005).

[11] P. Frymier, R. Ford, H. Berg, and P. Cummings, Proceedings of the National Academy of Sciences **92**, 6195 (1995).

[12] S. Umehara, I. Inoue, Y. Wakamoto, and K. Yasuda, Biophys. J. **93**, 1061 (2008).

[13] T. E. Kuhlman and E. C. Cox, Nucleic Acids Research **38**, e92 (2010).

[14] J. A. Sawitzke, L. C. Thomason, M. Bubunenko, X. Li, N. Costantino, and D. L. Court, *Recombineering: Highly Efficient in vivo Genetic Engineering using Single-strand Oligos*, 1st ed., Vol. 533 (Elsevier Inc., 2013).

[15] R. Lande, Evolution **33**, 402 (1979).

[16] R. G. Cox, J. Fluid Mech. **44**, 791 (1970).

[17] S. Taheri-Araghi, S. Bradde, J. T. Sauls, N. S. Hill, and P. A. Levin, Current Biology **25**, 385 (2015).